A recipe for desert : analysis of an extended Klausmeier model

Siero, E.P.J.A.

2 Beyond Turing: the response of patterned ecosystems to environmental change.

Spatially periodic patterns can be observed in a variety of ecosystems. Model studies revealed that patterned ecosystems may respond in a nonlinear way to environmental change, meaning that gradual changes result in rapid degradation. We analyze this response through stability analysis of patterned states of an arid ecosystem model. This analysis goes one step further than the frequently applied Turing analysis, which only considers stability of uniform states. We found that patterned arid ecosystems systematically respond in two ways to changes in rainfall: 1) by changing vegetation patch biomass or 2) by adapting pattern wavelength. Minor adaptations of pattern wavelength are constrained to conditions of slow change within a high rainfall regime, and high levels of stochastic variation in biomass (noise). Major changes in pattern wavelength occur under conditions of either low rainfall, rapid change or low levels of noise. Such conditions facilitate strong interactions between vegetation patches, which can trigger a sudden loss of half the patches or a transition to a degraded bare state. These results highlight that ecosystem responses may critically depend on rates, rather than magnitudes, of environmental change. Our study shows how models can increase our understanding of these dynamics, provided that analyses go beyond the conventional Turing analysis.

Appeared in Ecological Complexity in 2014 [180].

2.1 Introduction

Spatially periodic patterning of sessile biota can be observed in a variety of ecosystems including arid ecosystems [116], mussel beds [195], boreal peatlands [118] and tropical peatlands [11]. Such spatially periodic patterns can typically not be explained by underlying heterogeneity in the environment, which suggests that they are self-organized. Self-organization into periodic patterns is the result of positive feedbacks that act locally (short range activation) in combination with distal negative feedbacks (long range inhibition; [68]). This combination of feedbacks is also referred to as scale-dependent feedbacks [151]. In arid ecosystems, the combination of locally reduced evaporation through shading and water uptake by laterally extended roots is known to induce such scale-dependent feedbacks [70, 124]. Scale-dependent feedbacks can also result from the fact that in arid ecosystems plants tend to improve soil structure which allows more water to infiltrate during rain events [150, 186]. This results in increased water availability and increased plant growth, meaning that locally a positive feedback loop is active. However, water availability farther away is negatively affected by this facilitative effect: surface water accumulates on bare soils during intense rain events and moves towards vegetated areas due to a gentle slope or due to infiltration differences on flat terrain [97, 148]. In arid ecosystems, local positive feedbacks are therefore linked to a flux of resource that results in long range inhibition and consequently in pattern formation. This type of scale-dependent feedback is referred to as the resource-concentration mechanism [149]. The positive feedbacks that are often involved in pattern formation [151] are associated with nonlinear ecosystem response to environmental change [34, 149]. This means that gradual changes in environmental conditions may result in sudden significant losses in productivity and in degradation of patterned ecosystems.

Reaction-(advection-)diffusion models have been developed to understand the mechanisms responsible for pattern formation, to study the conditions under which scale-dependent feedbacks are strong enough for patterning to occur and to get more insight in the possible nonlinear behavior of patterned ecosystems, e.g. [70, 97, 148, 202]. In these models, patterns typically arise from a uniform system state that becomes unstable to heterogeneous perturbations. This type of instability is referred to as Turing instability (after A.M. Turing, 1912-1954; [190]) and is thought to be involved in for example the formation of patterns on animal coats [120], on sea shells [121] and

in chemical systems [74, 139]. Using linear stability analysis, it is possible to find the parameter ranges for which a uniform system state is Turing unstable.

At present, Turing analysis is used as a relatively simple way to study the environmental conditions under which one would expect periodic patterns to be observed, e.g. [61, 70, 79, 95, 97, 125]. However, since Turing analysis only considers the stability of uniform system states, it provides very little information about the behavior of ecosystems that are in a patterned state. Therefore, previous studies have been exploring this behavior using numerical approaches. These studies revealed a number of interesting properties of patterned ecosystems. Various model studies suggest that patterns can be expected under conditions where uniform system states are still stable and under conditions too harsh for uniform cover to be sustained, e.g. [148, 202]. These findings imply that stable uniform and stable patterned states can coexist for a range of environmental conditions [149]. The coexistence of alternative stable ecosystem states can result in so-called critical transitions [162] if environmental conditions change, which are associated with sudden losses of productivity and ecosystem degradation [164]. Numerical studies that looked in more detail to the dynamics of patterned ecosystem states suggest that multiple stable patterned states, with different wavelength or spatial configurations, can coexist and that this can result in hysteresis and more gradual ecosystem adaptation if environmental conditions change [16, 174].

Although studies with numerical approaches uncovered some interesting characteristics of patterned ecosystems, recent studies have been exploring whether the use of analytically based methods provides more detailed insights [172, 199]. These approaches go one step further than Turing analysis as they consider the stability of patterned rather than uniform ecosystem states. By combining stability analysis on patterned states with model runs, [172] demonstrated that hysteresis can be explained by the coexistence of multiple stable states. His study also suggests that the rate at which environmental conditions change may affect system response. This is of particular importance as current human activities induce anomalous rates of environmental change, e.g. [89]. Although these results suggest that information about the stability of patterned states is essential in understanding ecosystem response to changing environmental conditions, the application of stability analysis on patterned states in the field of ecology has been limited so far and various ecologically relevant questions remain to be answered [198, pp. 95-100].

One of the processes that are not well understood is the process of pattern wavelength adaptation. Patterned ecosystems can respond to environmental change by adapting pattern wavelength and the study by [172] showed that this process is affected by the rate of environmental change. It is, however, unknown why and how patterned ecosystems adapt and why this depends on the rate of change. In this study we therefore aim to provide a mechanistic understanding of how patterned ecosystems respond to environmental change, considering both the magnitude of change as well as the rate of change. By applying stability analysis on patterned system states, we first show that the use of Turing analysis can yield false negatives and false positives with regard to predicting the existence of observable (i.e. stable) patterns. Based on the mechanisms that are involved in pattern destabilization, we then discuss possible types of pattern adaptation. Using model runs, we demonstrate that knowledge about the stability of patterned states is crucial in understanding the response of ecosystems subject to environmental change and show how the rate of change in environmental conditions and the level of imposed spatio-temporal noise affect system response. Finally, we propose that competition for resources between patches of vegetation provides a possible ecological explanation for the obtained results. In this study we use an extended version of an arid ecosystem model by [97] as introduced by [199], which we will discuss in the next section.

2.2 Model description and analyses

2.2.1 Model description

The extended version of the Klausmeier model is a reaction-advection-diffusion model in which the formation of spatial vegetation patterns is the result of competition for surface water. The model has two state variables that are functions of both time t and space x ($x \in \mathbb{R}$): plant biomass n and surface water w. Notice that we will consider only one spatial dimension (x), following [199] and [172]. The model is given by equation (2.1) and (2.2). We use a non-dimensional version the model in order to reduce the number of parameters. For a dimensional version of the model and the physical

meaning of the parameters, see appendix 2.A.

$$\frac{\partial w}{\partial t} = a - w - wn^2 + v\frac{\partial w}{\partial x} + e\frac{\partial^2 w^\gamma}{\partial x^2} \tag{2.1}$$

$$\frac{\partial n}{\partial t} = wn^2 - mn + \frac{\partial^2 n}{\partial x^2} \tag{2.2}$$

The change in surface water w (equation (2.1)) is controlled by rainfall a, surface water losses (second term) and uptake by plants through infiltration and transpiration (third term). As in the original model by [97], the movement of surface water due to gradients in the terrain is captured with an advection term (fourth term). We extended the model by adding diffusion of surface water (fifth term). We did this for three reasons. First, the diffusion term has a physical basis as it can be derived from the shallow water equations [70]. Second, it allows us to capture the movement of surface water induced by spatial differences in infiltration rate [148]. Third, it enables us to demonstrate that the type stability analysis we use to study the system's response to change can be applied to both reaction-advection-diffusion and reaction-diffusion model ($v \neq 0$ and $v = 0$ respectively).

The dynamics in plant biomass n (equation (2.2)) are determined by plant growth which is linearly related to water uptake (first term) and by plant mortality (second term). As in the original model, plant dispersion is modeled with a diffusion term (third term).

The non-dimensional version of the model has five parameters. We chose parameter values that are valid for grass as reported by [97]. Plant mortality was set to $m = 0.45$ and for flat and sloped terrain $v = 0$ and $v = 182.5$ respectively. As we are interested in the response of the system to changes in rainfall, we use rainfall a as bifurcation parameter and let it vary between $a = 0$ to $a = 3.5$. For simplicity we chose $\gamma = 1$. [199] showed that the value of γ does not qualitatively affect the structure of stability regions. Therefore the results presented in the following sections are not expected to differ qualitatively for other values of γ. Finally, e was calibrated to obtain patterns in a realistic rainfall range according to studies listed by [37], which appeared to be for $e = 500$. For conversion of these dimensionless parameters to dimensional parameters, see appendix 2.A.

The extended Klausmeier model falls in the broader class of reaction-advection-diffusion models referred to as activator-depleted substrate systems [59] with vegetation being the activator and surface water being the substrate. In addition, it shows strong similarities with other well studied

models, depending on parameter choice. Naturally, if $e = 0$ we return to the original (one dimensional) Klausmeier model [97]. With $v = 0$ and $\gamma = 1$ the model is equal to the model studied by [94] and the well studied chemical model by [74]. Finally, the model has been studied by [199] for constant rainfall a.

It should be mentioned that apart from the model by [97] and derivations thereof [94, 199] a large body of model studies have been published that dedicate pattern formation in arid ecosystems to a variety of mechanisms, including competition for surface water [57,79,148], competition through soil water uptake by roots [125, 202], a combination of these mechanisms [70] or plant-plant interactions only [108–111]. These models may be suitable depending on system characteristics such as climate, soil and plant properties and can be used to answer specific research questions. However, here we limit our study to the analysis of the more generic extended Klausmeier model as it captures pattern formation in a relatively parsimonious way.

2.2.2 Analyses

In order to study the response of the system to changes in rainfall a, knowledge is required about the rainfall ranges for which stable spatially uniform and patterned states of equations (2.1) and (2.2) exist. We derived the existence of system states and assessed their stability by performing linear stability analysis. This type of analysis, together with the obtained stability regions in parameter space, will be discussed in detail in the next section. The boundaries of the stability regions were obtained by tracking the marginally stable patterned system states [51,171] using AUTO continuation software [41, AUTO-07p].

As the rainfall a changes stable states may lose their stability. The stability regions, as obtained using stability analysis, provide insight in when a system state destabilizes. However, the behavior of the system after destabilization (e.g. re-stabilization) is a priori unknown. To study this, we performed runs of the model with linearly increasing and decreasing rainfall a. The model runs were performed in MATLAB (version 2012a - 7.14.0.739; The MathWorks, Inc.) using a vector of 1024 elements that represent a domain with a size of 1000 (500 meters). Periodic boundary conditions were used to diminish boundary effects and to mimic an infinite domain. We studied the response of the system under different rates of change in a ($\frac{da}{dt} = -10^{-7}$, -10^{-4} and -10^{-2}). We added spatially and temporally

uncorrelated multiplicative uniformly distributed noise to both components of the model every $\frac{1}{4}$ year (noise amplitude = 0, $5{\cdot}10^{-5}$% and 0.05%). The noise was added to diminish numerical artifacts, such as the system residing in unstable system states, and represents potential sources of noise that are not captured by the deterministic equations.

The state of the system can be expressed in terms of pattern wavenumber κ ($= \frac{2\pi}{\text{wavelength}}$). To enable comparison between the model runs and the stability regions, we assessed the wavenumber of the patterns as generated by the model by applying discrete Fourier transformations. This is explained in detail in appendix 2.B.

2.3 Stability of uniform and patterned states: from Turing instability to the Busse balloon

In this section we discuss the stability of uniform and patterned states of the extended Klausmeier model. In subsection 2.3.1 we briefly review well-known linear stability analysis (Turing analysis) as applied to uniform system states. We then continue by discussing the mathematically more challenging stability analysis of patterned states in subsection 2.3.2. Finally we compare the stability regions obtained in both subsections and discuss the ecologically relevant results in subsection 2.3.3.

2.3.1 Existence and stability of uniform system states

Determining the stability of uniform steady states to uniform perturbations is a fairly easy task: first one derives the steady states of the system, and then one perturbs the steady states. The stability of the system state is then defined by the sign of the exponential growth rate of the perturbation: the maximum real part of eigenvalues λ. Solely negative real parts of eigenvalues imply a (asymptotically) stable state, whereas a positive real part means that the system state is unstable. A bifurcation occurs when due to a parameter change the growth rate of a perturbation $\max(\mathrm{Re}(\lambda))$ becomes positive (here max() refers to the maximum of a set values and Re() takes the real part of a complex number). The system is marginally stable at such an onset of instability. Marginal stability marks the boundaries of stability regions in parameter space.

Uniform system states can be derived by setting equations (2.1) and (2.2)

to zero while neglecting advection and diffusion fluxes. The extended Klausmeier model presented in the previous section has three uniform steady states for $a > 2m$ (see appendix 2.D.1 for a derivation). Two of the steady states are vegetated (so $\bar{n} > 0$), of which one is stable to uniform perturbations for ecologically relevant parameter values ($m < 2$) and one is unstable (see appendix 2.D.2 for stability analysis). A stable bare desert state ($\bar{n} = 0$) exists for all values of a. At $a = a_{SN} := 2m$ a saddle-node bifurcation occurs. Here the vegetated states cease to exist, meaning that for $a < a_{SN}$ only a stable bare state exists.

Perturbations in natural systems are generally heterogeneous. To account for this in the stability analysis, spatially heterogeneous perturbations can be added to the uniform states [59, 190]. Heterogeneous perturbations can be represented as sinusoids with wavenumber κ ($= \frac{2\pi}{\text{wavelength}}$) of which the amplitude grows (or decays) with a rate of $\max(\text{Re}(\lambda(\kappa)))$.

When perturbing the stable uniformly vegetated state of the extended Klausmeier model with such sinusoids (appendix 2.D.3), a range of values for a can be found for which the state is Turing unstable. Here the amplitude of a perturbing sinusoid grows over time ($\max(\text{Re}(\lambda(\kappa, a))) > 0$). Whether this occurs does not only depend on intrinsic model parameters, such as a, but also on the wavenumber of the sinusoid κ. The solid red line in figure 2.1a,b borders the region in (a, κ)-space for which the uniformly vegetated state is Turing unstable. Assuming that the amplitude of the imposed perturbations grow while their wavenumber is preserved, one would expect patterns to exist in this region. Therefore this can be seen as a *Turing prediction region*. If rainfall decreases over time, patterns will form directly after the Turing bifurcation T [199, or Turing-Hopf bifurcation TH if $v \neq 0$] as here the uniform state becomes unstable. These patterns will have a wavenumber close to κ_T (or κ_{TH}): the wavenumber of the perturbation that initializes the Turing bifurcation. Model runs show that when randomly perturbing uniform states that are Turing unstable, the system tends to evolve to a state with a pattern wavenumber close to the wavenumber of the perturbation with the largest growth rate, also referred to as most unstable mode (dashed red line in figure 2.1a,b; [174]). As we will show in section 2.4 however, pattern wavenumber can strongly deviate from the this wavenumber if environmental conditions change.

2.3.2 Existence and stability of patterned system states

So far we have discussed the stability of uniform system states. The patterned states that arise from a Turing unstable uniform state are, however, not necessarily stable themselves. Unlike uniform steady states, it is generally not possible to find explicit expressions for patterned states by hand. For this and subsequent determination of stability we rely on numerics.

Patterns may exist in the form of so-called *wavetrains*: vegetation bands that slowly migrate in uphill direction. In fact for $v = 182.5$ this is the case for all patterns. To deal with this a comoving frame $\xi = x - st$ is introduced. Here s is equal to the migration speed: a pattern dependent property that is assumed to be constant in space and time. This results in additional advection terms in both equations. A pattern (w_p, n_p) with wavenumber κ exists for rainfall a if and only if it is a solution to the system

$$0 = a - w_p - w_p n_p^2 + (v + s)\frac{dw_p}{d\xi} + e\frac{d^2 w_p^\gamma}{d\xi^2} \tag{2.3}$$

$$0 = w_p n_p^2 - m n_p + s\frac{dn_p}{d\xi} + \frac{d^2 n_p}{d\xi^2} \tag{2.4}$$

on the domain $[0, \frac{2\pi}{\kappa}]$ with periodic boundary conditions. See appendix 2.E.1 for a derivation of these equations. Notice that, besides the parameters of the extended Klausmeier model (equations (2.1) and (2.2)), migration speed s and wavenumber κ now appear as additional parameters. Parameters s and κ can be used to express the state of the system.

Since the existence of unstable patterned states is not of immediate interest we also require stability. To determine this we need to linearize about (w_p, n_p) leading to ordinary differential equations with a dependency on w_p and n_p (appendix 2.E.2). The perturbations are no longer represented by sinusoidals. Instead they are given by products of two functions: a sinusoidal $e^{i\nu}$ (with wavenumber ν) and an a priori unknown periodic function with the same wavenumber κ as the pattern. The eigenvalues of the corresponding perturbations are complex and depend on ν.

Stable patterns exist in what is referred to as the *Busse balloon* (after F.H. Busse; [21]): the region in (parameter,κ)-space for which at least one stable periodic solution exists [199]. If a patterned state is stable, it is said to be in the Busse balloon. Busse balloons for the extended Klausmeier model are depicted in figure 2.1a,b (bordered by the black solid line). Apart from the

patterned states, a stable uniform bare state ($\kappa = 0$) exists for all rainfall values.

Stability regions are bordered by marginally stable solutions. Therefore a Busse balloon can be constructed by finding marginally stable solutions. If one marginally stable solution is known it is possible to track marginal stability while changing a parameter (with the use of continuation software AUTO; [41]). A precise description of this procedure can be found in the article by [147]. The Busse balloon is obtained by plotting the wavenumbers κ of the marginally stable solutions against the changing parameter. In order to track marginal stability we also need to know exactly how the eigenvalues obtain a positive real part: what is the destabilization mechanism?

In [199] it is rigorously proven through the derivation of amplitude equations (Ginzburg-Landau analysis) that stable patterns exist close to the Turing(-Hopf) bifurcation: it is derived that the bifurcation is supercritical (for the scalings considered). Close to the Turing(-Hopf) bifurcation the region in (a, κ)-space where stable patterns exist is bounded by a parabola of marginally stable patterns [199]. Also, the destabilization mechanism is identified as being a *sideband instability* or *Eckhaus instability*.

The sideband instability is characterized by a change in sign of the curvature of the eigenvalues attached to the origin ($\nu = 0$), as depicted in figure 2.1c. For marginally stable patterns, which separate stable from unstable patterns, there is no curvature at $\nu = 0$. This corresponds to a second derivative at $\nu = 0$ that equals zero. If, due to changing rainfall, patterns lose their stability, perturbations with ν close (but unequal) to zero become able to destabilize patterned states.

With the current parameter combination the sideband is the dominant destabilization mechanism for the extended Klausmeier model [199]. Only for very small wavenumbers κ it is superseded by intertwining Hopf instabilities [51]. In this case, onset of instability occurs away from $\nu = 0$, but continuation with AUTO is still possible [51, 147].

The perturbations, which consist of products of $e^{i\nu}$ and functions with the same wavenumber as the pattern κ, need not be periodic, but can be for particular values of ν. For example, perturbations with $\nu = 0$ are periodic with pattern wavenumber κ, since $e^0 = 1$. As shown in figure 2.1c, perturbations with wavenumber κ ($\nu = 0$) are not able to destabilize a patterned state: due to translation symmetry the growth rates of these perturbations remain zero. Perturbations with $\nu = \pi$ are periodic with wavenumber $\kappa/2$

since $e^{\pi i} = -1$. If perturbations with wavenumber $\kappa/2$ ($\nu = \pi$) become able to destabilize a patterned state, a so-called spatial *period doubling bifurcation* occurs. Growth of these perturbations results in a halving of the pattern wavenumber. Recall that the wavelength is inversely proportional to the wavenumber, so the wavelength (spatial period) doubles. According to figure 2.1c, perturbations of this kind are the last to destabilize a patterned state as rainfall a decreases, however they do attain the largest growth rate soon after. The black dashed line in figure 2.1a,b depicts the period doubling instability.

In summary, we discussed that the stability of patterned states can be assessed by tracking marginal stability. To do this, knowledge about the destabilization mechanisms is required. For the extended Klausmeier model the sideband instability is the dominant destabilization mechanism, meaning the curvature (second derivative) of the curve of eigenvalues (figure 2.1c) can be used to trace the boundary of the stable pattern region.

2.3.3 Ecological implications

We determined the stability of patterned ecosystem states and discussed some important destabilization mechanisms, but what ecologically relevant information can we extract from figure 2.1?

First, we observe that the Turing prediction region and the Busse balloon only partly overlap. A large part of the patterns in the Turing prediction region turn out to be unstable, and are therefore unlikely to observed. Furthermore, stable patterns exist outside the Turing prediction region for $a < a_{SN}$ and if $v \neq 0$, also for $a > a_{SN}$. These patterns cannot form directly from a Turing unstable uniform state. Although stable patterns do no appear at rainfall values above the Turing(-Hopf) bifurcation for the extended Klausmeier model, this may be different for other models, e.g. [148]. The differences between the Turing prediction region and the Busse balloon suggest that a relatively simple Turing analysis gives very limited information about the parameter regimes for which one can expect patterns to be observed.

Second, figure 2.1 shows that for a given rainfall value a range of stable patterned states exists. Since the system has many stable states, it can be considered *multistable*. The current state, in terms of wavenumber κ, consequently depends on history, meaning that hysteresis can be expected.

Third, a pattern with a given wavenumber κ is stable for a range of a. This means that the same pattern wavenumber can in theory be observed for

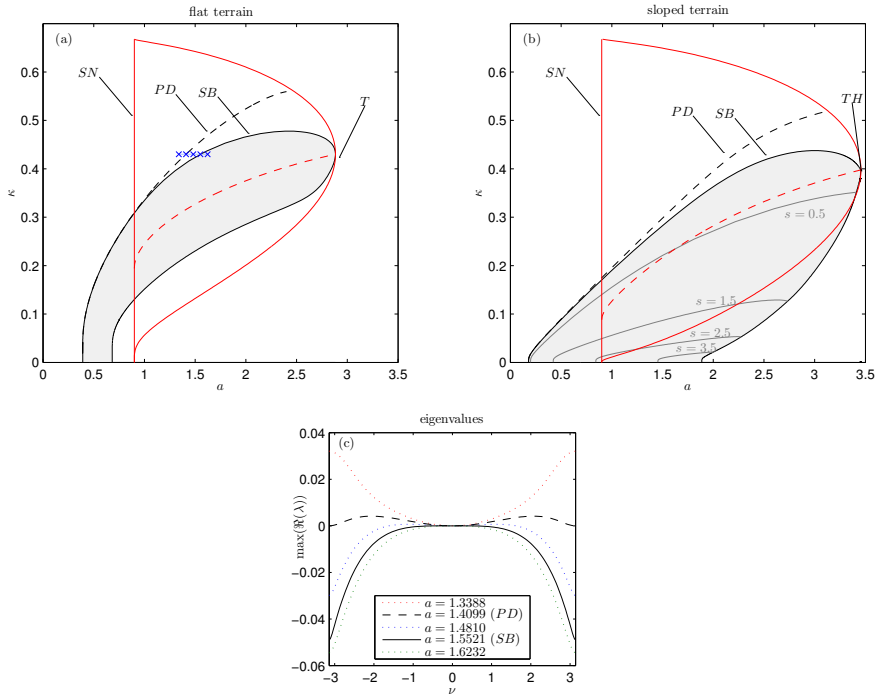

Figure 2.1: Stability regions of the non-dimensional extended Klausmeier model (equations (2.1) and (2.2)) in (a, κ)-space for flat (a; $v = 0$) and sloped terrain (b; $v = 182.5$). In (a) and (b) a represents rainfall and κ is the wavenumber of the patterned state. The black solid curve indicates the location of the sideband instability and borders the stable pattern region or Busse balloon (shaded area). A period doubling bifurcation occurs on the black dashed line. The grey curves in (b) show the contours of constant uphill pattern migration speed s. The red solid line borders the Turing prediction region where perturbations of the uniformly vegetated state grow in amplitude. On the right hand border of the Turing prediction region uniform states are marginally stable to spatial perturbations. On the left hand border of this region the Turing unstable uniform state ceases to exist (saddle-node bifurcation SN; $a = a_{SN} := 2m$). The wavenumber of the perturbation with the largest growth rate is indicated by the red dashed line. The highest rainfall value at which the uniformly vegetated state is Turing unstable is marked as the Turing bifurcation point T (or Turing-Hopf bifurcation point TH if $v \neq 0$). (c) The maximum real part of eigenvalues for perturbations of patterned states plotted against Floquet wavenumber ν. The perturbed patterned states have a wavenumber of $\kappa = 0.43009$ ($\approx \kappa_T$). Notice that the perturbed states are marked with crosses in (a). At $a \approx 1.5521$ a sideband bifurcation (SB) occurs. Here the curvature at $\nu = 0$ changes sign. At $a \approx 1.4099$ a period doubling bifurcation (PD) occurs. Here $\max(\mathrm{Re}(\lambda(\nu)))$ at $\nu = \pi \approx 3.14$ becomes positive.

a range of external conditions. Furthermore, if external conditions change, one would expect the wavenumber of a pattern to remain constant as long as it is stable, i.e. as long as the external conditions remain within the range for which the pattern is stable.

Fourth, the shape of the Busse balloon allows high wavenumbers to be stable only at high values of a. The opposite is true for low wavenumbers. The presence of a slope affects the shape of the Busse balloon. Pattern formation occurs at higher rainfall rates and patterned states can sustain under more arid conditions on sloped terrains. The absence of a slope allows high wavenumber patterns to be stable, while the rainfall range for which stable low wavenumber patterns exist is narrow. On sloped terrains in contrast low wavenumber patterns can be expected to be observed for a wide rainfall range.

Finally, we observe that the period doubling instability approaches the boundary of the Busse balloon as rainfall a decreases. Meaning that at low rainfall values, period doubling takes place almost simultaneously with the destabilization of a pattern. In addition, the boundary of the Busse balloon is steeper at low rainfall values. This means that at low rainfall values an incremental decline in rainfall could result in desertification if the system is close to the boundary of the Busse balloon.

2.4 System response to changing environmental conditions

The obtained information about the stability and destabilization of patterned states is not enough to fully understand the behavior of patterned ecosystems when subject to changing environmental conditions. This is because the linearization we implicitly apply only enables us to describe the behavior of the system close to the steady state. Consequently, if the system is pushed away from a steady state (during pattern destabilization) it is a priori unknown to which state it will evolve (restabilization). In this section we study the behavior of the system while gradually changing the rainfall parameter and relate this behavior to the findings presented in the previous section. First we describe history dependence within the system resulting from multistability in subsection 2.4.1. In subsection 2.4.2 we then study in more detail the restabilization of the system and its dependence on the rate with which rainfall changes and on the level of noise imposed on the system.

Finally, in subsection 2.4.3 we propose an ecological mechanism that controls system restabilization.

2.4.1 Bouncing through the Busse balloon

The non-dimensional extended Klausmeier model (equations (2.1) and (2.2)) was run with the rainfall a changing over time with a rate of $\frac{da}{dt} = \pm 10^{-4}$. This rate of change corresponds to a change in annual rainfall of about 0.1 mm year^{-1}.

Figure 2.2 shows how the system responds to changing rainfall on flat terrain ($v = 0$). When rainfall decreases, patterns in plant biomass emerge shortly after the uniformly vegetated state becomes Turing unstable (figure 2.2a). The mean plant biomass of the patterned state does not differ much from that of the Turing unstable uniform system state (figure 2.2d). The wavenumber of the pattern does not change as long as the pattern is stable. The pattern amplitude in contrast increases during pattern formation after which it slowly decreases with declining a. At some point, the decreasing rainfall forces the system outside the Busse balloon and the pattern destabilizes (figure 2.2c). This results in a pattern with a lower wavenumber and a larger amplitude. These transitions are not distinguishable in mean biomass (figure 2.2d). The adaptation of the wavenumber is accompanied by the extinction of what can be considered as vegetation patches. When a reaches a value for which no stable patterned state exists, desertification occurs and all remaining patches go extinct simultaneously.

If rainfall increases over time similar behavior can be observed (figure 2.2b), however now patterns destabilize at the lower border of the Busse balloon and the wavenumber increases until eventually a uniformly vegetated state is reached (figure 2.2c). During wavenumber adaptation vegetation patches split up. Since the trajectories for decreasing and increasing rainfall differ, hysteresis occurs [172].

On sloped terrain (figure 2.3), patterns emerge in the form of vegetation bands that migrate in uphill direction (traveling waves). As the Busse balloon is wider in terms of wavenumber κ the hysteresis effect is more pronounced when compared to flat terrain. As shown by figure 2.3, the migration speed of the vegetation bands gets lower as rainfall decreases. However, during wavenumber adaptation vegetation bands accelerate leading to slightly elevated migration speeds directly after transition.

Although wavenumber adaptation occurs some time after patterned states

destabilize, as discussed earlier by [172], figures 2.2 and 2.3 indicate that the Busse balloon helps in understanding how patterned ecosystems respond to changes: 1) as long as the system is in the Busse balloon it responds by changing the amplitude (and migration speed) of the patterns, 2) if, due to changing rainfall a, the system is forced outside the Busse balloon it responds by changing its pattern wavenumber.

At first sight, the Busse balloon does not seem to provide insight in what determines the selection of a new wavenumber after pattern destabilization. In the next section we show how wavenumber selection is affected by the rate at which the rainfall changes and by the amount of spatio-temporal noise to which the system is exposed.

2.4.2 Wavenumber selection: the role of rate of change and noise

The model was run for $v = 0$ with different rates of change in rainfall $\left|\frac{da}{dt}\right|$ (with $\frac{da}{dt} < 0$) and different noise levels. As shown in figure 2.4, wavenumber adaptation occurs with increasing step size (in terms of wavenumber κ) for increasing rates of change. At high rates of change, desertification can take place at rainfall levels for which stable patterned states still exist. For the level of noise imposed on the system, the opposite is true: higher noise levels result in smaller step size. At sufficiently high noise levels, patches go extinct one-by-one and the system tends to closely follow the boundary of the Busse balloon.

We observe that during some wavenumber adaptations period doubling occurs, meaning that half of the vegetation patches go extinct simultaneously [207]. The occurrence of period doubling is related to the position of the system in (a, κ)-space at which the wavenumber adaptation is initiated, which is in turn determined by rate of change and noise level. If wavenumber adaptation takes place close to the boundary of the Busse balloon, which is the case for low rates of change or high noise levels, period doubling does not occur. If wavenumber adaptation is initiated farther away from the boundary of the Busse balloon, period doubling occurs, provided that the system surpassed the period doubling instability PD and that period doubling results in a stable patterned solution.

At low rainfall values we find that period doubling occurs more frequently (even at high noise levels). Here the period doubling instability PD approaches the sideband instability SB (boundary of the Busse balloon). As a result the period doubling instability PD is surpassed even at low rates of

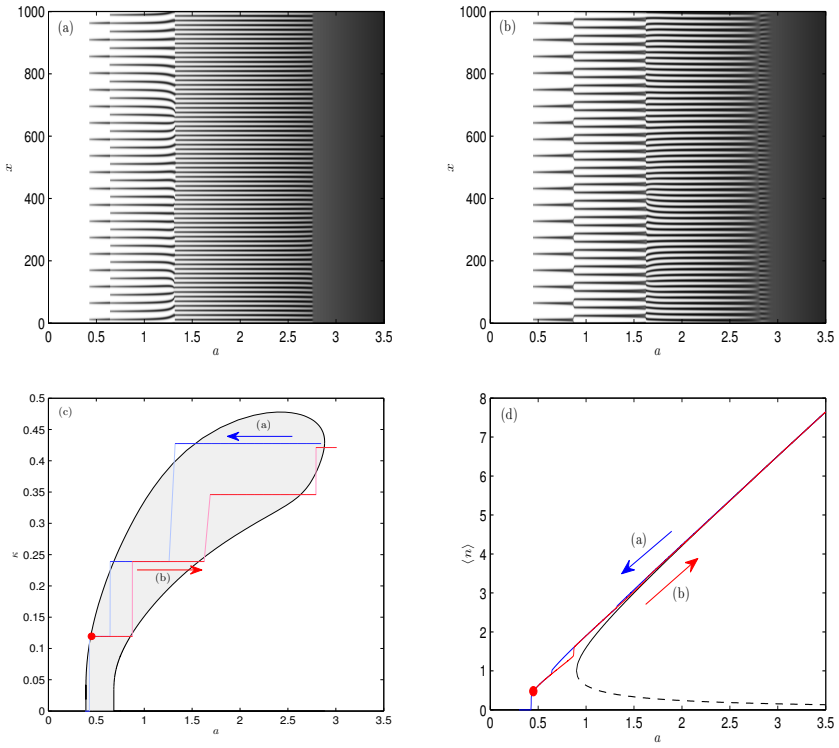

Figure 2.2: Plant density n in space for runs of the non-dimensional extended Klausmeier model with $v = 0$ (flat terrain), for $\frac{da}{dt} = -10^{-4}$ (a) and $\frac{da}{dt} = 10^{-4}$ (b). The former run starts from the homogeneously vegetated steady state. The latter is initiated with the patterned solution of the first at $a = 0.45$. Spatially and temporally uncorrelated multiplicative uniformly distributed noise with an amplitude of $5{\cdot}10^{-5}\%$ is added to the plant density every $\frac{1}{4}$ year. The trajectories through the Busse balloon in (c) were obtained by applying a discrete Fourier transformation with respect to x (see appendix 2.B). In (d), the mean biomass is plotted for both runs. The solid and dashed black lines are the uniform steady states.

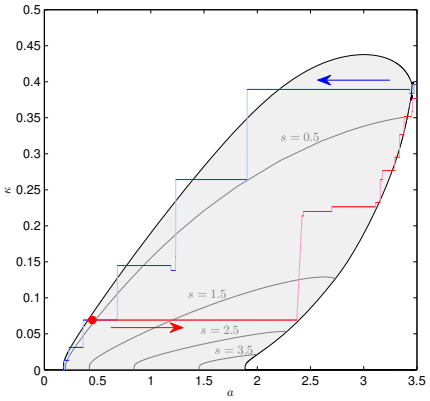

Figure 2.3: See the caption of figure 2.2, but now $v = 182.5$ (sloped terrain). The grey curves show the contours of constant uphill pattern migration speed.

change.

2.4.3 Competition between and rearrangement of patches

In the previous subsections we showed that wavenumber adaptation driven by changing environmental conditions can be a discontinuous process: many patches can go extinct simultaneously if a pattern destabilizes. In addition, we found that rainfall, the rate of change in rainfall and the level of noise on the system affect the number of patches that go extinct. Here we provide an interpretation of the observed system responses by taking a closer look to what happens during wavenumber adaptation.

Figure 2.5 shows plant biomass and surface water for part of the modeled domain during one of the wavenumber adaptations in a model run with declining rainfall. The figure shows that the extinction of one vegetation patch results in growth of its neighboring patches, which in turn negatively affects their neighbors. This triggers a cascade, eventually resulting in extinction of half of the patches.

The interaction between neighboring patches in the extended Klausmeier model can be explained by the competition for water. Vegetation patches harvest water from an area bordered by water divides where $\frac{dw}{dx} = 0$. The uptake of water by patches that share a water divide, which is controlled by patch biomass, determines the position of the water divide. An increase

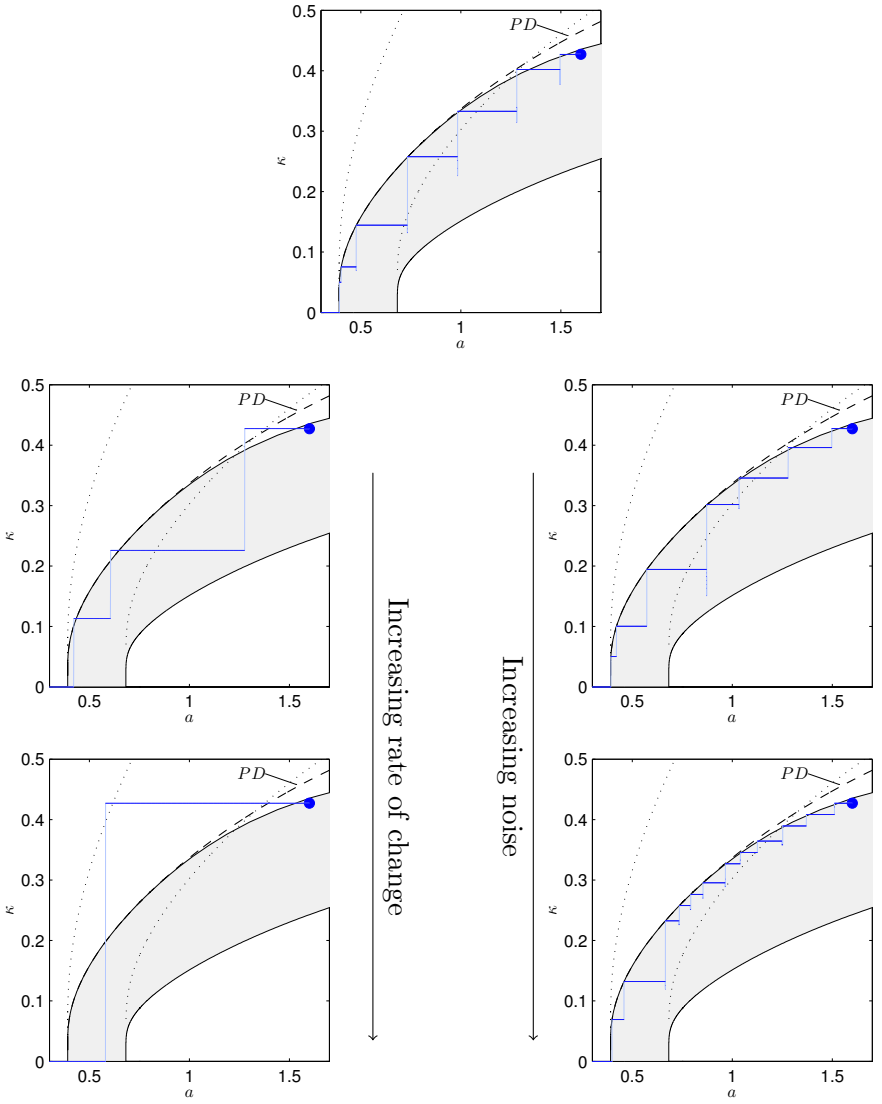

Figure 2.4: Trajectories through the Busse balloon for runs with decreasing rainfall and with different rates of change in a and different noise levels. The trajectories were obtained by applying a discrete Fourier transformation with respect to x (see appendix 2.B). The runs were initiated with a stable pattern solution at $\kappa \approx \kappa_T$ and $a = 1.6$ and end in the desert state $\kappa = 0$. The solid line depicts the sideband instability SB, the dashed line is the period doubling instability PD. The area bordered by the dotted curves was extrapolated from the Busse balloon and depicts the area in which period doubling would result in a stable patterned solution. The top panel plus the two panels on the left have no noise, the rate of change in rainfall $\left|\frac{da}{dt}\right|$ changes respectively from 10^{-7} to 10^{-4} to 10^{-2}. The two panels on the right have noise amplitude $5 \cdot 10^{-5}\%$ (upper) and 0.05% (lower) while the rate of change of a is equal to that of the top panel (10^{-7}).

in patch biomass with respect to neighboring patches will widen the water harvesting area of a patch. The opposite occurs if a patch is weaker than its neighbors. Since the water harvesting area affects water availability, it feeds back to patch biomass eventually resulting in growth or extinction of a patch.

We observe (figure 2.6) that wavenumber adaptations during which less than half of the vegetation patches goes extinct are accompanied by rapid spatial rearrangement of patches, while no movement of patches can be observed if half (period doubling) or all patches go extinct (desertification). The movement of neighboring patches during rearrangement seems to weaken the feedbacks described above: if one patch goes extinct its neighboring patches fill up the created space, thereby diminishing the stress on remaining patches.

Patch rearrangement generally occurs if wavenumber adaptation is initiated between the sideband instability and the period doubling instability. At low rainfall values, the period doubling instability approaches the sideband instability. At these rainfall values rearrangement of patches becomes less likely, as pattern destabilization almost coincides with the period doubling instability PD. High rates of change in rainfall also do not allow for patch rearrangement. High noise levels in contrast can trigger wavenumber adaptation before the system crosses the period doubling instability PD, resulting in patch rearrangement and one-by-one extinction of vegetation patches.

2.5 Discussion and conclusions

In this study we showed that patterned ecosystems systematically respond in two ways to changing environmental conditions: 1) by adjusting patch biomass (pattern amplitude) or 2) by changing pattern wavelength (wavenumber). In the latter case patches go extinct or split up and may rearrange. In arid ecosystems, gradual wavelength adaptation is constrained to conditions of high rainfall, slow changes in rainfall and high levels of stochastic spatial variation in biomass (noise). The adaptation process is less gradual under conditions of either low rainfall, rapid change or low levels of noise. Such conditions do not allow vegetation patches to rearrange, and facilitate the simultaneous extinction of half the patches or even a transition to a degraded state without any patches.

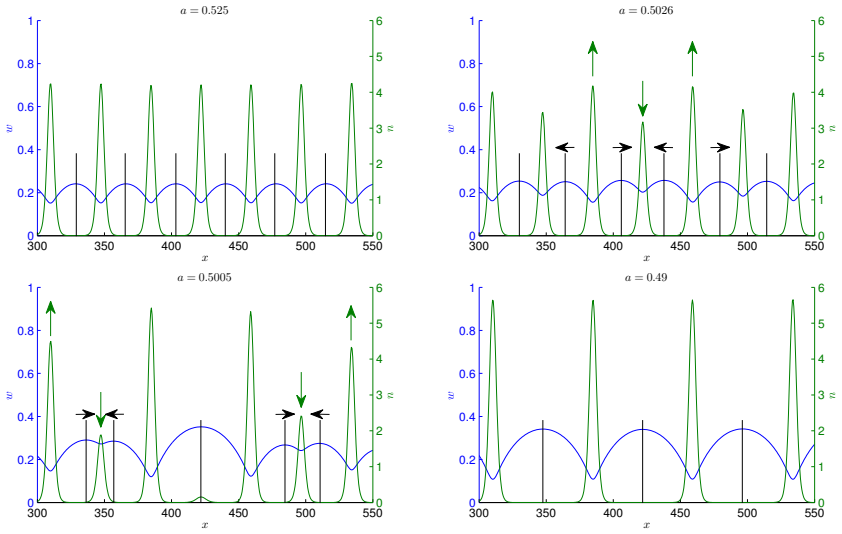

Figure 2.5: Plant biomass n and water w against space x, for $v = 0$ and $\frac{da}{dt} = -10^{-4}$. The black lines mark the position of water divides. The black arrows indicate the direction of the movement of the water divides. The green arrows indicate the growth or decay in n.

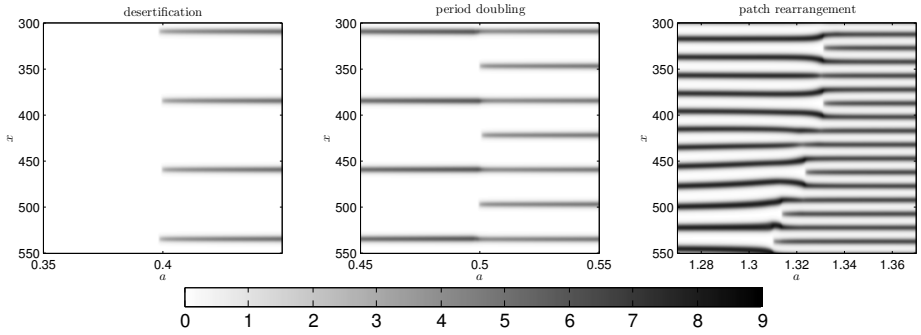

Figure 2.6: Plant density n in space x against rainfall a during different wavenumber adaptations in a model run with declining rainfall. Rearrangement of patches during a transition only occurs at high rainfall values. At low rainfall patches do not rearrange promptly and period doubling or desertification occurs.

We found that an overview of stable patterned states, the Busse balloon, is a powerful tool in understanding the response of patterned ecosystems to changing environmental conditions. If a system is in a stable patterned state (i.e. in the Busse balloon), a pattern tends to solely adapt its amplitude, while if the system leaves the Busse balloon, a pattern adapts its wavenumber. The ability of patches to rearrange is determined by the period doubling instability. Once the system surpasses this instability, patches do not rearrange, leading to extinction of half or all the patches.

Our findings suggest that the response of patterned ecosystems to environmental change does not only depend on the magnitude of change, but also on the rate with which conditions change: patterned ecosystems may not be able to respond in a gradual way to rapid environmental change. Similar behavior can be observed in a number of non-spatial models, e.g. [113, 165]. Nonlinear response to rapid environmental change may as well occur in more comprehensive models that are used for policy making. This may imply that merely setting targets for tolerable change may not be sufficient to prevent ecosystem degradation and that to ensure gradual ecosystem adaptation, identification of critical rates of change is required as well.

Besides the rate of change in environmental conditions, the level of noise to which the system is exposed seems to play an essential role in ecosystem response. Our study shows that relatively small amplitude noise brings heterogeneity in the population of patches which leads to more gradual ecosystem adaptation to environmental change. Larger amplitude noise, on the other hand, is known to be a cause of critical transitions [83].

Our findings are in agreement with a recent study by [39] based on areal images of patterned vegetation in Sudan. Like [39] we found that pattern wavenumber declines with increasing aridity and that, when compared to flat terrain, a wider range of pattern wavenumbers can be found on sloped terrain. Although our stability analysis suggest that low wavenumber patterns are stable (and thus can be observed in theory), [39] did not find such patterns. This might be explained by the fact that, at least for flat terrain, low wavenumber patterns are stable only for a relatively small rainfall range (figure 2.1a). A second explanation can be found in the steepness of the boundary of the Busse balloon. Wavenumber adaptation forced by environmental changes generally results in increased ecosystem resilience as it increases the distance to critical thresholds (the boundary of the Busse balloon). However, if the boundary of the Busse balloon is steep, as is the case for low wavenumber patterns at low rainfall values (figure 2.1a), the

system remains close to the boundary of the Busse balloon meaning that the increase in ecosystem resilience is relatively small. As a result patterned arid ecosystems are relatively fragile in this parameter region. Variations in seasonal and annual precipitation, to which all arid ecosystems are exposed, can easily trigger desertification. Consequently, low wavenumber patterns are less likely to be observed.

By assessing the existence and stability of patterned system states we went one step further than Turing analysis, frequently applied in previous studies, e.g. [61, 70, 79, 95, 97, 125]. In a wide range of ecosystems, scale-dependent feedbacks are thought to involve local positive feedbacks [151]. Such local positive feedbacks allow stable patterned states to exist under conditions where uniform cover can no longer be sustained. Analysis of patterns in these parameter regions is of importance because of proximity to critical thresholds. Using conventional Turing analysis, however, it is fundamentally impossible to do so. The novel approach we presented in this paper is a promising way forward in understanding the behavior of spatially explicit ecosystem models under these conditions.

The findings presented in this paper are in accordance with previous model studies. Analysis of the original Klausmeier model by [174] and [172] already suggested the existence of patterned states in parameter regions where Turing unstable states are absent, see also [148], and that hysteresis can occur in pattern wavenumber and migration speed. In contrast to the study by [172] we used wavenumber as state variable instead of migration speed. In practice, wavenumber is a property that is easier to assess than migration speed [30, 38]. In addition, migration speed cannot be used as state variable if all patterns are stationary. This is the case on flat terrain in the extended Klausmeier model, but on sloped terrain patterns can be fixed as well [58, 185]. The existence of a multitude of stable patterned states has been demonstrated in other models as well [16, 124, 172, 208]. In this paper we showed that transitions between stable patterned states can be forced by changing environmental conditions. Previous studies show that such transitions can also be triggered by disturbances in the form of the uniform biomass removal [124] or patch removal [208].

Although our findings seem to be in line with observations [39], most findings remain to be tested using areal images and field data. Empirical proof for a Busse balloon requires a constant pattern wavelength to be observed for a range of environmental conditions or, alternatively, a range of pattern wavelengths to be observed for a fixed set of environmental conditions. It

would also be interesting to see if competition between neighboring patches indeed occurs and how the competition strength depends on environmental stress. If time series of areal images are available, it may also be possible to observe hysteresis in pattern wavelength.

To get more insight in the behavior of real ecosystems we propose that future studies apply stability analysis on patterned system states of other (more realistic) models. Constructing Busse balloons for other models will allow to relate findings to measurable parameters. Stability analysis of models in which multiple pattern forming mechanisms are captured, such as the model by [70], would allow studying how the relative strength of these mechanisms affects the global behavior of patterned ecosystems [96]. In addition, future studies could consider two spatial dimensions as this may qualitatively affect the model behavior described in this paper. Accounting for more than one spatial dimension in stability analysis is mathematically challenging, since more complex spatial patterns can evolve (gaps, labyrinths and spots; [139, 148]) and more destabilization mechanisms may potentially destabilize a patterned system state [85]. Finally, as soon as bare ground forms between patches, the movement and stability of patches can be described by pulse interaction, see [48, 184] and references therein. This may provide insight in the ecologically relevant process of wavenumber adaptation forced by environmental change.

The changes in climate projected for the coming decades [86] are likely to affect the functioning of patterned ecosystems worldwide. We showed that in order to understand the behavior of patterned ecosystems that are subject to change, mathematical techniques are required that go beyond conventional Turing analysis. By assessing the stability of patterned ecosystem states and by studying the relevant destabilization mechanisms we were able to explain when and how arid ecosystems may adapt their pattern wavelength. Identification of the Busse balloon, together with the period doubling instability, provides a theoretical framework for future theoretical and empirical studies. These studies may provide enhanced insights in the response of other ecological models to change, the response of real ecosystems to change, and the ecological mechanisms responsible for this response.

Acknowledgments

This study is supported by a grant within the Complexity program of the Netherlands Organization of Scientific Research (NWO). The research of MR is also supported by funding from the European Union's Seventh Framework Programme (FP7/2007-2013) under grant agreement no. 283068 (CASCADE).

2.A A non-dimensional extended Klausmeier model.

The extended Klausmeier model is given by equation (2.A.1) and (2.A.2). In table 2.1, the values of the parameters are listed for both grass and trees, as estimated by [97]. The diffusion term was calibrated to obtain patterns in a realistic parameter range. A non-dimensional version of the model (equation (2.A.3) and (2.A.4)) is used throughout the paper. Table 2.2 shows how the dimensionless parameters can be obtained.

$$\frac{\partial W}{\partial T} = A - LW - RWN^2 + V\frac{\partial W}{\partial X} + E\frac{\partial^2 W^\Gamma}{\partial X^2} \tag{2.A.1}$$

$$\frac{\partial N}{\partial T} = RJWN^2 - MN + D\frac{\partial^2 N}{\partial X^2} \tag{2.A.2}$$

$$\frac{\partial w}{\partial t} = a - w - wn^2 + v\frac{\partial w}{\partial x} + e\frac{\partial^2 w^\gamma}{\partial x^2} \tag{2.A.3}$$

$$\frac{\partial n}{\partial t} = wn^2 - mn + \frac{\partial^2 n}{\partial x^2} \tag{2.A.4}$$

2.B Wavenumber plotting by fast Fourier transform

In this appendix we explain how we compute the trajectories through (parameter,κ)-space, as depicted in the main text, by using the discrete or *fast Fourier transform*.

In the model runs the plant biomass $n(x)$ is represented by a vector $n(j)$, $j = 1, 2, ..., N$, of $N = 1024$ elements and the spatial domain size is $L = 1000$. The vector can be expressed as a linear combination of vectors $v_l(j) = e^{\frac{2\pi i l}{N} j}$, where $l = 0, 1, 2, ..., N-1$. The v_l represent sinusoidals with wavenumber

Table 2.1: Values and units for the variables and parameters of the extended Klausmeier model (equation (2.A.1) and (2.A.2)). Values adopted from [97]. E was calibrated to obtain patterns in a realistic parameter range, according to [37].

Parameter/Variable	Value (grass)	Value (tree)	Unit
W			kg m^{-2}(=mm)
N			kg m^{-2}
X			m
T			year
A	0 - 950	0 - 950	kg m^{-2} $year^{-1}$ (= mm $year^{-1}$)
L	4	4	$year^{-1}$
R	100	1.5	kg m^{-2} $year^{-1}$ kg^{-2} (=mm $year^{-1}$ kg^{-2})
V	0 or 365	0 or 365	m $year^{-1}$
E	500	500	m^2 $year^{-1}$ $mm^{1-\Gamma}$
Γ	1	1	-
J	0.003	0.002	kg kg^{-1} (=kg L^{-1})
M	1.8	0.18	$year^{-1}$
D	1	1	m^2 $year^{-1}$

Table 2.2: Physical meaning and values for the variables and parameters of the non-dimensional extended Klausmeier model (equation (2.A.3) and (2.A.4))

Parameter/Variable	Physical meaning	Value (grass)	Value (tree)
w	$WR^{1/2}L^{-1/2}J$	$0.015W$	$0.0012W$
n	$NR^{1/2}L^{-1/2}$	$5N$	$0.61N$
x	$XL^{1/2}D^{-1/2}$	$2X$	$2X$
t	TL	$4T$	$4T$
a	$AR^{1/2}L^{-3/2}J$	$0.00375A$	$0.0003062A$
m	ML^{-1}	$0.25M$	$0.25M$
v	$VL^{-1/2}D^{-1/2}$	$0.5V$	$0.5V$
e	ED^{-1}	E	E
γ	Γ	Γ	Γ

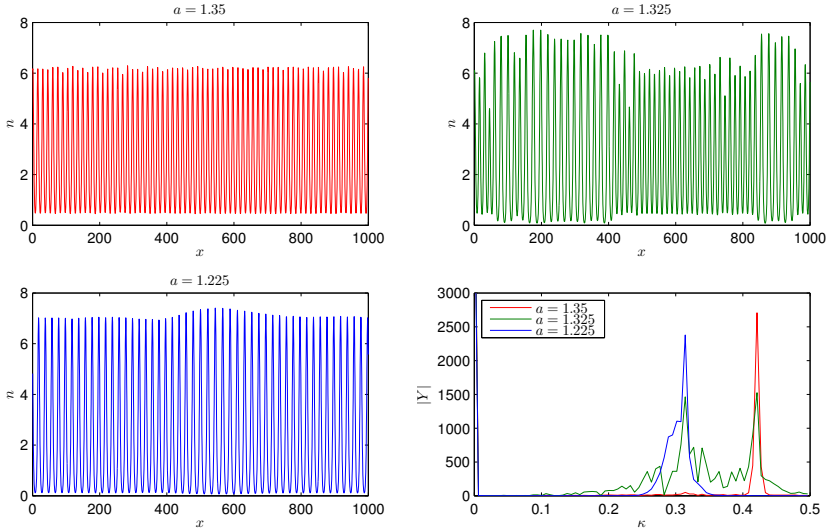

Figure 2.7: Plant biomass n against space x before, during and after wavenumber adaptation in the model run with declining rainfall of figure 2.2 and the Fourier transform of the corresponding vectors.

$\kappa = \frac{2\pi l}{L}$. The weight of v_l in n can be computed by the discrete Fourier transform

$$Y(\kappa) = \sum_{j=1}^{N} n(j) v_l(-j). \tag{2.B.1}$$

The absolute value of $Y(\kappa)$ is a measure of how much n resembles a sinusoidal with wavenumber κ. If a single $Y(\kappa)$ has a large absolute value compared to all other Y ($\kappa \neq 0$), then the state is (nearly) periodic with wavenumber κ.

The trajectories through (parameter,κ)-space, as depicted in the main text, were obtained by picking the wavenumber where $|Y|$ attained its maximum, $\kappa = 0$ excluded. The wavenumber is only plotted when the maximum is relatively large, which suppresses plotting during transient dynamics.

Figure 2.7 shows that during wavenumber adaptation the spread in κ increases. After wavenumber adaptation the spread decreases slowly. As the pattern settles, the maximum wavenumber can still change. As l is an integer, κ can only attain certain values. Therefore the settling of the pattern can result in small jumps in pattern wavenumber.

2.C General equations for perturbations.

We derive equations for perturbations of a general system state in the extended Klausmeier model. These equations will be of use in appendix 2.D.2, 2.D.3 and 2.E.2. For ease of the computations we restrict to the linear diffusion case $\gamma = 1$. Let (w, n) be a system state that is perturbed by (w', n'). We obtain an expression for the governing equations of the perturbation by the following calculations:

$$\begin{aligned}
\frac{\partial w'}{\partial t} =& \frac{\partial (w + w')}{\partial t} - \frac{\partial w}{\partial t} \\
=& e\frac{\partial^2 (w + w')}{\partial x^2} + v\frac{\partial (w + w')}{\partial x} + a - (w + w') - (w + w')(n + n')^2 \\
& - \left(e\frac{\partial^2 w}{\partial x^2} + v\frac{\partial w}{\partial x} + a - w - wn^2 \right) \\
=& e\frac{\partial^2 w'}{\partial x^2} + v\frac{\partial w'}{\partial x} - w'(1 + n^2) - 2n'wn - 2w'n'n - n'^2 w - w'n'^2 \\
\approx& e\frac{\partial^2 w'}{\partial x^2} + v\frac{\partial w'}{\partial x} - w'(1 + n^2) - 2n'wn \qquad (2.C.1) \\
\frac{\partial n'}{\partial t} =& \frac{\partial (n + n')}{\partial t} - \frac{\partial n}{\partial t} \\
=& \frac{\partial^2 (n + n')}{\partial x^2} + (w + w')(n + n')^2 - m(n + n') \\
& - \left(\frac{\partial^2 n}{\partial x^2} + wn^2 - mn \right) \\
=& \frac{\partial^2 n'}{\partial x^2} + w'n^2 + n'(2wn - m) + 2w'n'n + n'^2 w + w'n'^2 \\
\approx& \frac{\partial^2 n'}{\partial x^2} + w'n^2 + n'(2wn - m) \qquad (2.C.2)
\end{aligned}$$

The final approximate equalities are equalities in a linear approximation: for small perturbations (w', n') the products $w'n'$ and n'^2 are negligible.

In an abstract formulation equations (2.C.1) and (2.C.2) can be rewritten as:

$$\frac{\partial}{\partial t} \begin{pmatrix} w' \\ n' \end{pmatrix} = A \begin{pmatrix} w' \\ n' \end{pmatrix} \qquad (2.C.3)$$

where the so-called spectrum, a generalization of the concept of eigenvalues,

of the differential operator

$$A = \begin{pmatrix} e\frac{\partial^2}{\partial x^2} + v\frac{\partial}{\partial x} - 1 - n^2 & -2wn \\ n^2 & \frac{\partial^2}{\partial x^2} + 2wn - m \end{pmatrix} \tag{2.C.4}$$

determines the stability of (w, n).

2.D Analysis of the homogeneous steady states.

For completeness we will give a thorough analysis of the homogeneous steady states of the extended Klausmeier model. This also serves the purpose of showing how easily results can be obtained by hand in this case, compared to the restricted possibilities for the analysis of patterns in appendix 2.E. The results of section 2.D.1 and 2.D.2 also hold for $\gamma = 2$.

2.D.1 Existence of spatially homogeneous steady states

If w and n are spatially homogeneous, gradients in w and n are absent, and the advection-diffusion terms of (2.1) and (2.2) vanish. Since only a single type of derivative remains, the partial differential equations become ordinary differential equations. The steady uniform states can then be found by solving (2.D.1) and (2.D.2).

$$\frac{dw}{dt} = a - w - wn^2 = 0 \tag{2.D.1}$$

$$\frac{dn}{dt} = wn^2 - mn = (wn - m)n = 0 \tag{2.D.2}$$

Clearly $\bar{n}_B = 0$ solves (2.D.2) and consequently $\bar{w}_B = a$. This is a bare desert state, as plant biomass equals zero. Alternatively (2.D.2) is solved if $n = \frac{m}{w}$. Substituting this in (2.D.1) and multiplying with $-w$ we obtain the quadratic equation $w^2 - aw + m^2 = 0$. This quadratic equation can be solved to obtain two solutions for w and from $n = \frac{m}{w}$ the corresponding solution

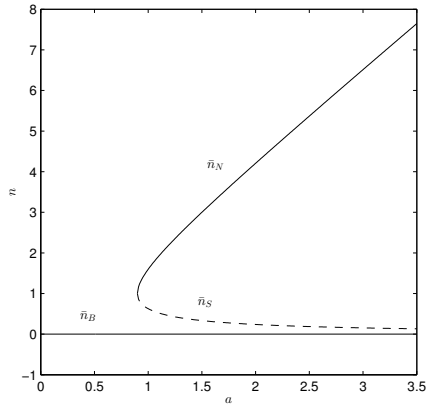

Figure 2.8: Homogeneous steady states of the (extended) Klausmeier model expressed in plant biomass n as function of rainfall a for $m = 0.45$.

for n can be computed. The outcome is given by:

$$\bar{w}_S = \frac{2m^2}{a - \sqrt{a^2 - 4m^2}} \tag{2.D.3}$$

$$\bar{n}_S = \frac{a - \sqrt{a^2 - 4m^2}}{2m} \tag{2.D.4}$$

$$\bar{w}_N = \frac{2m^2}{a + \sqrt{a^2 - 4m^2}} \tag{2.D.5}$$

$$\bar{n}_N = \frac{a + \sqrt{a^2 - 4m^2}}{2m} \tag{2.D.6}$$

Here the argument of the square root needs to be positive, so these states only exist for $a \geq 2m$. Note that the two states coincide at $a = 2m$, in fact here a so-called saddle-node bifurcation takes place. In the following subsection we will show that $(\bar{w}_S, \bar{n}_S)$ has a stable and an unstable direction (saddle, unstable) and $(\bar{w}_N, \bar{n}_N)$ either has two stable or unstable directions (node). Note that we have covered all possible cases of (2.D.2) and thus no other homogeneous steady states can exist. Moreover, all the steady states are non-negative. We will continue by studying their stability.

2.D.2 Stability of the homogeneous steady states against homogeneous perturbations

By perturbing the steady states obtained in appendix 2.D, their stability can be determined. If a perturbation grows over time, the steady state is unstable. The steady state is stable, if all perturbations decay. In this appendix, we show how linear stability analysis can be used to assess the stability of uniform system states to homogeneous perturbations. We will do this by using the equations derived for perturbations in appendix 2.C.

Since perturbations are assumed to be homogeneous (2.C.1) and (2.C.2) simplify to:

$$\frac{\partial w'}{\partial t} = - w'(1+\bar{n}^2) - 2\bar{n}' w\bar{n} \tag{2.D.7}$$

$$\frac{\partial n'}{\partial t} = w'\bar{n}^2 + n'(2\bar{w}\bar{n} - m) \tag{2.D.8}$$

This can be compactly written as:

$$\begin{pmatrix} \frac{dw'}{dt} \\ \frac{dn'}{dt} \end{pmatrix} = \begin{pmatrix} -1-\bar{n}^2 & -2\bar{w}\bar{n} \\ \bar{n}^2 & 2\bar{w}\bar{n} - m \end{pmatrix} \begin{pmatrix} w' \\ n' \end{pmatrix} \tag{2.D.9}$$

where the matrix is readily identified as the Jacobian matrix J of the reaction terms. As is well-known, the stability can be determined by looking at the real parts of the eigenvalues of the Jacobian.

For the bare state plugging in $\bar{n}_B = 0$ in the Jacobian matrix yields

$$J = \begin{pmatrix} -1 & 0 \\ 0 & -m \end{pmatrix}. \tag{2.D.10}$$

The eigenvalues can now be read of from the diagonal ($\lambda_1 = -1$, $\lambda_2 = -m$) so the bare state is always stable (for $m > 0$).

In case of the saddle-node states we recall that $nw = m$ (appendix 2.D.1). So the Jacobian matrix becomes

$$J = \begin{pmatrix} -1-\bar{n}_{S,N}^2 & -2m \\ \bar{n}_{S,N}^2 & m \end{pmatrix}. \tag{2.D.11}$$

The eigenvalues can be computed directly by solving the characteristic equation involving the determinant det:

$$\begin{aligned} \det(J - \lambda I) =& \det \begin{pmatrix} -1-\bar{n}^2-\lambda & -2m \\ \bar{n}^2 & m-\lambda \end{pmatrix} \\ =& \lambda^2 + \lambda(1+\bar{n}^2-m) - m + m\bar{n}^2 = 0 \end{aligned} \tag{2.D.12}$$

Solving this we obtain:

$$\lambda_{\pm} = -\frac{1}{2}\left(1+\bar{n}^2-m\right) \pm \sqrt{m\left(1-\bar{n}^2\right)+\frac{1}{4}\left(1+\bar{n}^2-m\right)^2} \tag{2.D.13}$$

Which has the form:

$$\lambda_{\pm} = \alpha \pm \sqrt{\beta+\alpha^2} \tag{2.D.14}$$

For this general form it holds:

	$\beta > 0$	$\beta < 0$
$\alpha > 0$	$\mathrm{Re}(\lambda_+) > 0$	$\mathrm{Re}(\lambda_+) > 0$
	$\mathrm{Re}(\lambda_-) < 0$	$\mathrm{Re}(\lambda_-) > 0$
$\alpha < 0$	$\mathrm{Re}(\lambda_+) > 0$	$\mathrm{Re}(\lambda_+) < 0$
	$\mathrm{Re}(\lambda_-) < 0$	$\mathrm{Re}(\lambda_-) < 0$

(2.D.15)

We first show that $(\bar{w}_S, \bar{n}_S)$ has both a stable and an unstable direction (saddle, unstable), as was claimed in appendix 2.D.1. For this it suffices to show that $\beta = m(1-\bar{n}_S^2) > 0$. Since $a > 2m$ (appendix 2.D.1)

$$\bar{w}_S = \frac{2m^2}{a-\sqrt{a^2-4m^2}} = \frac{2m^2\left(a+\sqrt{a^2-4m^2}\right)}{a^2-a^2+4m^2} = \frac{a}{2}+\frac{1}{2}\sqrt{a^2-4m^2} > m \tag{2.D.16}$$

Now $\bar{n}_S = \frac{m}{\bar{w}_S} < 1$ so $\beta > 0$.

Second we show that $(\bar{w}_N, \bar{n}_N)$ is a node (i.e. is either stable or unstable in both directions), as was claimed in appendix 2.D.1, but we will not directly determine the stability. This is equivalent to $\beta = m(1-\bar{n}_N^2) < 0$. Since $a > 2m$ we have

$$\bar{n}_N = \frac{a+\sqrt{a^2-4m^2}}{2m} = \frac{a}{2m}+\frac{1}{2m}\sqrt{a^2-4m^2} > 1 \tag{2.D.17}$$

So indeed $\beta < 0$.

Finally the eigenvalues belonging to the node can have positive (unstable) or negative (stable) real parts. Both eigenvalues are negative if and only if $\alpha = -\frac{1}{2}(1+\bar{n}_N^2-m) < 0$, this is automatically satisfied if $m < 1$, so in particular if $m = 0.45$. For general m it can be calculated that the stability boundary is given by pairs (m, a) that satisfy:

$$a = \frac{m^2}{\sqrt{m-1}} \text{ and } m \geq 2 \tag{2.D.18}$$

This boundary is plotted in figure 2.9.

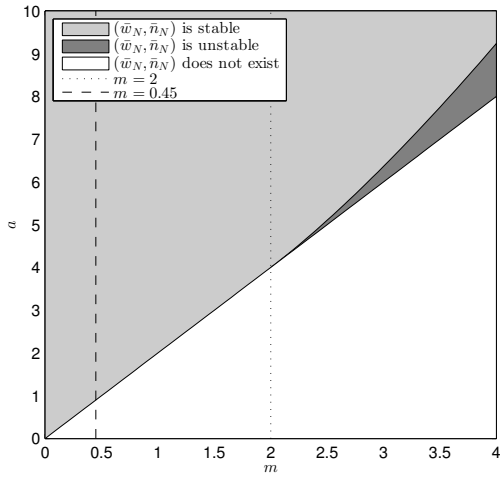

Figure 2.9: Region in parameter space where $(\bar{w}_N, \bar{n}_N)$ is stable, unstable or does not exist.

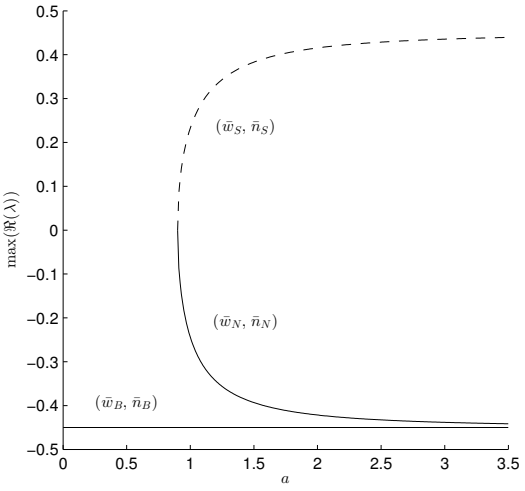

Figure 2.10: The maximum real part of λ for the spatially uniform steady states plotted against a. Perturbations are assumed to be spatially homogeneous and $m = 0.45$.

2.D.3 Turing analysis of the steady states

In the full model the steady states are also subject to heterogeneous perturbations. States that were thought of as being stable against homogeneous perturbation may be unstable against a wider class of perturbations. For simplicity we restrict to $\gamma = 1$.

The usual approach is to assume that the spatial dependence of the perturbation has the form of a sinusoid: we represent it by a complex exponential $e^{i\kappa x}$.[1] This is convenient because $\frac{d}{dx}e^{i\kappa x} = i\kappa e^{i\kappa x}$ and $\frac{d^2}{dx^2}e^{i\kappa x} = -\kappa^2 e^{i\kappa x}$. Substituting

$$\begin{pmatrix} w'(t,x) \\ n'(t,x) \end{pmatrix} = e^{i\kappa x}\begin{pmatrix} \tilde{w}(t) \\ \tilde{n}(t) \end{pmatrix} \tag{2.D.19}$$

in (2.C.1) and (2.C.2) and dividing by $e^{i\kappa x}$ yields:

$$\frac{\partial \tilde{w}}{\partial t} = -\kappa^2 e\tilde{w} + i\kappa v\tilde{w} - \tilde{w}(1+n^2) - 2\tilde{n}wn \tag{2.D.20}$$

$$\frac{\partial \tilde{n}}{\partial t} = -\kappa^2\tilde{n} + \tilde{w}n^2 + \tilde{n}(2wn - m) \tag{2.D.21}$$

This can be written in a single matrix equation:

$$\begin{pmatrix} \frac{d\tilde{w}}{dt} \\ \frac{d\tilde{n}}{dt} \end{pmatrix} = \begin{pmatrix} -\kappa^2 e + i\kappa v - 1 - \bar{n}^2 & -2\bar{w}\bar{n} \\ \bar{n}^2 & -\kappa^2 + 2\bar{w}\bar{n} - m \end{pmatrix}\begin{pmatrix} \tilde{w} \\ \tilde{n} \end{pmatrix} \tag{2.D.22}$$

The justification of the assumption that the perturbation is sinusoidal is given by the Fourier transform, which links the spectrum of the operator A in the abstract formulation (2.C.3) to the eigenvalues of the above matrix.

For the bare state $\bar{n}_B = 0$, so the matrix simplifies to

$$\begin{pmatrix} -\kappa^2 e + i\kappa v - 1 & 0 \\ 0 & -\kappa^2 - m \end{pmatrix} \tag{2.D.23}$$

so $\lambda_1 = -\kappa^2 e + i\kappa v - 1$ and $\lambda_2 = -\kappa^2 - m$. Since the real parts $\mathrm{Re}(\lambda_1) = -\kappa^2 e - 1$ and $\mathrm{Re}(\lambda_2) = -\kappa^2 - m$ both remain negative for any κ, the bare state is also stable against heterogeneous perturbations. Because the saddle is already unstable against homogeneous perturbations we focus our attention on the node. Since $\bar{w}_N\bar{n}_N = m$ the matrix becomes

$$\begin{pmatrix} -\kappa^2 e + i\kappa v - 1 - \bar{n}_N^2 & -2m \\ \bar{n}_N^2 & -\kappa^2 + mi \end{pmatrix}, \tag{2.D.24}$$

[1] If there are only second order spatial derivatives present, assuming the form $\cos(\kappa x)$ or $\sin(\kappa x)$ is equivalent.

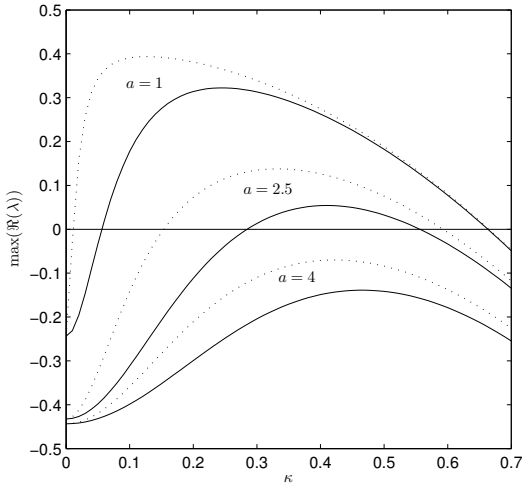

Figure 2.11: The maximum real part of λ for heterogeneous perturbations of $(\bar{w}_N, \bar{s}_N)$, plotted as function of κ, for different values of a and for $v = 0$ (solid lines) and $v = 182.5$ (dotted lines), $m = 0.45$. The boundary of the Turing prediction region depicted in figure 2.1 is located at the intersection points of the curves with the x-axis. The maxima of the curves correspond to the most unstable wavenumber.

from which we can obtain the eigenvalues by solving the dispersion relation:

$$\det \begin{pmatrix} -\kappa^2 e + i\kappa v - 1 - \bar{n}_N^2 - \lambda & -2m \\ \bar{n}_N^2 & -\kappa^2 + m - \lambda \end{pmatrix} = 0 \qquad (2.D.25)$$

This again yields a quadratic equation in λ, which can be solved for λ. The eigenvalues λ are now not only a function of model parameters, but also a function of wavenumber κ. Figure 2.11 shows solutions of (2.D.25) (which depends on a through $\bar{n}_N$) for several values of a for $m = 0.45$. The curves pass through the real axis between $a = 4$ and $a = 2.5$ in both the case $v = 0$ and $v = 182.5$, the node becomes Turing unstable somewhere in between (precise values are given in the caption of figure 2.1).

2.E Analysis of patterns

In the previous appendix all of the analysis could be done by hand. This is very much in contrast to the analysis of patterns. Here we give some results that can be obtained analytically for the extended Klausmeier model.

2.E.1 Existence of patterns

Here we derive that patterns are solutions of the equations (2.3) and (2.4). These equations are solved numerically.

In general, patterned states may migrate uphill (if $v \neq 0$). We will denote the migration speed (in the direction of increasing x) of these so-called wavetrains by s. Allowing for $s = 0$, any pattern can be written in the form $(w(t,x), n(t,x)) = (w_p(x-st), n_p(x-st)) = (w_p(\xi), n_p(\xi))$, where w_p and n_p are periodic functions describing the wave profile and $\xi = x - st$ is a comoving frame coordinate. By using the chain rule, e.g.

$$\frac{\partial w(x,t)}{\partial t} = \frac{dw_p(\xi)}{d\xi}\frac{\partial \xi}{\partial t} = -s\frac{dw_p}{d\xi} \tag{2.E.1}$$

after substituting the forms in (2.1) and (2.2) we obtain

$$0 = a - w_p - w_p n_p^2 + (v+s)\frac{dw_p}{d\xi} + e\frac{d^2 w_p^\gamma}{d\xi^2} \tag{2.E.2}$$

$$0 = w_p n_p^2 - m n_p + s\frac{dn_p}{d\xi} + \frac{d^2 n_p}{d\xi^2} \tag{2.E.3}$$

which are the equations we set out to find.

2.E.2 Stability of patterns

We will study the stability of a pattern $(w(t,x), n(t,x))$ in the case $\gamma = 1$, so the equations for the perturbation (2.C.1) and (2.C.2) hold. We show these equations again, now with explicit dependence on the coordinates:

$$\begin{aligned}\frac{\partial w'(t,x)}{\partial t} =& e\frac{\partial^2 w'(t,x)}{\partial x^2} + v\frac{\partial w'(t,x)}{\partial x} - w'(t,x)\left(1 + n(t,x)^2\right) \\ & - 2n'(t,x)w(t,x)n(t,x)\end{aligned} \tag{2.E.4}$$

$$\begin{aligned}\frac{\partial n'(t,x)}{\partial t} =& \frac{\partial^2 n'(t,x)}{\partial x^2} + w'(t,x)n(t,x)^2 \\ & + n'(t,x)\left(2w(t,x)n(t,x) - m\right)\end{aligned} \tag{2.E.5}$$

Here w and n are not constant, which prevents us from applying a sinusoidal substitution as in Turing analysis (appendix 2.D.3). As in appendix 2.E.1 we write $(w(t,x), n(t,x)) = (w_p(\xi), n_p(\xi))$ with $\xi = x - st$. To make optimal use of this form we apply a change of coordinates $(t,x) \mapsto (t,\xi)$. Simultaneously we substitute $(w', n') = e^{\lambda t}(\tilde{w}(\xi), \tilde{n}(\xi))$ and after division by $e^{\lambda t}$ we obtain:

$$\lambda\tilde{w} = e\frac{d^2\tilde{w}}{d\xi^2} + (v+s)\frac{d\tilde{w}}{d\xi} - \tilde{w}(1+n_p^2) - 2\tilde{n}w_p n_p \tag{2.E.6}$$

$$\lambda\tilde{n} = \frac{d^2\tilde{n}}{d\xi^2} + s\frac{d\tilde{n}}{d\xi} + \tilde{w}n_p^2 + \tilde{n}(2w_p n_p - m) \tag{2.E.7}$$

This is a system of two second order ordinary differential equations. After defining $\tilde{q} = \frac{d\tilde{w}}{d\xi}$ and $\tilde{r} = \frac{d\tilde{n}}{d\xi}$ it can be rewritten as a first order system of four ordinary differential equations:

$$\frac{d}{d\xi}\begin{pmatrix}\tilde{w}\\ \tilde{q}\\ \tilde{n}\\ \tilde{r}\end{pmatrix} = \begin{pmatrix} 0 & 1 & 0 & 0 \\ \frac{\lambda+1+n_p^2}{e} & \frac{-v-s}{e} & \frac{2w_p n_p}{e} & 0 \\ 0 & 0 & 0 & 1 \\ -n_p^2 & 0 & m-w_p n_p & -s \end{pmatrix}\begin{pmatrix}\tilde{w}\\ \tilde{q}\\ \tilde{n}\\ \tilde{r}\end{pmatrix} \tag{2.E.8}$$

Since the matrix of coefficients is periodic, we are ready to use Floquet theory. Through Floquet theory it is possible to express the spectrum as the union of curves of eigenvalues of a related problem. The spatial part of the perturbations that act as eigenfunctions satisfy:

$$\tilde{w}\left(\xi + \frac{2\pi}{\kappa}; \nu\right) = e^{i\nu}\tilde{w}(\xi;\nu) \tag{2.E.9}$$

$$\tilde{n}\left(\xi + \frac{2\pi}{\kappa}; \nu\right) = e^{i\nu}\tilde{n}(\xi;\nu) \tag{2.E.10}$$

where κ is now the pattern wavenumber and $\nu \in (-\pi, \pi]$. Note that $\frac{2\pi}{\kappa}$ is the wavelength of the pattern. A corresponding curve of eigenvalues was exhibited as a function of ν in figure 2.1c, for different values of a. Regarding the stability we will not go into more details but note that the procedure for assessing stability is explained further in [147].

A special case is when $\nu = \pi$. Then $e^{i\nu} = -1$. It follows that $\tilde{w}(\xi + \frac{4\pi}{\kappa}; \pi) = -\tilde{w}(\xi + \frac{2\pi}{\kappa}; \pi) = \tilde{w}(\xi; \pi)$, and similarly for $\tilde{n}$, so the perturbation has twice the wavelength of the pattern. When the real part of the corresponding eigenvalue becomes positive, the pattern can be destabilized by such a perturbation and the period will be doubled (period doubling instability).